N94- 29655

TDA Progress Report 42-116 February 15, 1994

Enhanced Orbit Determination Filter Sensitivity Analysis: Error Budget Development

J. A. Estefan
Navigation Systems Section

P. D. Burkhart
The University of Texas at Austin

An error budget analysis is presented which quantifies the effects of different error sources in the orbit determination process when the enhanced orbit determination filter, recently developed, is used to reduce radio metric data. The enhanced filter strategy differs from more traditional filtering methods in that nearly all of the principal ground system calibration errors affecting the data are represented as filter parameters. Error budget computations were performed for a Mars Observer interplanetary cruise scenario for cases in which only X-band (8.4-GHz) Doppler data were used to determine the spacecraft's orbit, X-band ranging data were used exclusively, and a combined set in which the ranging data were used in addition to the Doppler data. In all three cases, the filter model was assumed to be a correct representation of the physical world. Random nongravitational accelerations were found to be the largest source of error contributing to the individual error budgets. Other significant contributors, depending on the data strategy used, were solar-radiation pressure coefficient uncertainty, random Earth-orientation calibration errors, and Deep Space Network (DSN) station location uncertainty.

I. Introduction

Development of improved navigation techniques which utilize radio Doppler and ranging data acquired from NASA's Deep Space Network (DSN) have received considerable study in recent years, as these data types are routinely collected in tracking, telemetry, and command operations. Furthermore, the availability of high-speed workstation computers has made possible the use of computationally intensive data processing modes for reducing all radio metric data. A new sequential data filtering strategy currently under study is the *enhanced orbit determination filter*, in which most if not all of the major systematic ground system calibration error sources are treated as filter (estimated) parameters, along with the spacecraft trajectory parameters. This strategy differs from the current practice, in which the ground system calibration error sources are represented as unestimated bias parameters, accounted for only when computing the error covariance of the filter parameters.

The motivation behind the enhanced filter is not so much to improve upon the a priori ground system calibrations, but to incorporate a more accurate model of the physical world into the filter [1]. Previous studies suggest that medium-to-high navigation accuracies (40 to 15 nrad in an angular sense) are achievable when the enhanced orbit determination filter is used in conjunction with X-band (8.4-GHz) Doppler and ranging [2]. Studies are also being conducted to demonstrate the utility of this new filtering strategy with actual flight data acquired from the Galileo spacecraft.[1] Critical to understanding the potential benefits and/or deficiencies of this type of orbit determination filter is the development of an *error budget*, which catalogs the contributions of a particular error source or group of error sources to the estimation errors. This form of sensitivity analysis identifies the major sources of error and where future work may need to be focused in order to improve overall navigation system performance.

This article first reviews the fundamental concepts of reduced-order filtering theory, which are essential for sensitivity analysis and error budget development. The theory is then applied to the development of an error budget for a Mars Observer interplanetary cruise scenario in which the enhanced orbit determination filter is used to reduce X-band Doppler and ranging data. The trajectory characteristics of this scenario are reviewed along with the data-acquisition strategies. The filter model is described and error budgets are given for three different data strategies: X-band Doppler only, X-band ranging only, and X-band Doppler plus ranging. For this initial study, the filter model is assumed to be a correct representation of the physical world.

II. Reduced-Order Filtering

In some navigation applications, it is not practical to implement a full-order or truly optimal filter when the system model, with all major error and noise sources, is of high order. This is often the case in applications such as a multisensor avionics navigation system, in which there are memory limitations in the onboard flight computer.[2] Moreover, it is implicitly assumed in the development of the filter equations that exact descriptions of the system dynamics, error statistics, and the measurement process are known; unfortunately, this is rarely true in practice [3]. Use of *reduced-order filtering* techniques allows the analyst to obtain estimates of key parameters of interest, with reduced computational burden and with moderate complexity in the filter model [3,4]. Thus, reduced-order, or, *suboptimal*, filters are the result of design trade-offs in which the designer performs a sensitivity analysis to determine which sources of error are most critical to overall system performance.

In general, the spacecraft orbit determination process is executed entirely on the ground and thus flight computer memory limitations are not a significant factor. Nevertheless, there are reasons for not always using a full-order optimal filter for spacecraft orbit determination. Some of the reasons include: (1) certain parameters, such as fiducial station locations, may be held fixed in order to define a reference frame and/or length scale; (2) there may be a lack of adequate models for an actual physical effect; (3) the existence of computational limitations when attempting to adjust parameters of high order, such as the coefficients in a gravity field; or (4) if estimated, the computed uncertainty in model parameters would be reduced far below the level warranted by model accuracy [5,6].

A. Filter Evaluation Modes

There are a number of error analysis methods which can be used to evaluate filter models and predict filter performance. Reduced-order error analysis techniques enable an analyst to study the effects of using incorrect a priori statistics, data-noise/data-weight assumptions, or process noise models on the filter design. This is usually referred to as the *general filter evaluation mode* and accomplished by establishing a fully detailed reference model (a *truth* model) against which the behavior of a filter can be compared [5]. If the filter is optimal, then the filter and truth models coincide. If the filter is suboptimal, then the filter model is of equal or lower order (i.e., reduced-order) than the truth model and possibly (but not necessarily) represents a subset of the states of the truth model [3]. In practice, a fully detailed truth model may be difficult to develop and thus one typically evaluates a range of "reasonable" truth models to assess whether the filter results are especially sensitive to a particular element(s) of the filtering strategy being used [5]. The objective is to design a filter model to achieve the best possible accuracy, but which is also robust, so that its performance will not be adversely affected by the use of slightly incorrect filter parameters. In the design process, the filter structure and the truth model remain fixed while repeated adjustments are made to the a priori statistics, data noise

[1] S. Bhaskaran (personal communication), Navigation Systems Section, Jet Propulsion Laboratory, Pasadena, California, October 1993.

[2] J. Vagners, *Development of the Minimum Variance Reduced Order (MVRO) Estimator Equations in Upper Triangular-Diagonal (U-D) Factored Form*, Boeing report D229-10602-1 (internal document), The Boeing Company, Seattle, Washington, February 21, 1979.

values, or process noise values, until acceptable behavior is achieved [4].

In a special case of reduced-order error analysis, often referred to as a *consider state analysis*, various systematic error sources are treated as unmodeled parameters which are not estimated, but whose effects are accounted for (i.e., "considered") in computing the error covariance of the estimated parameters [7].[3] In a consider state analysis, the sensitivity of the estimated parameter set to various unmodeled consider parameters can be computed via the partial derivatives of the state estimate with respect to the consider parameter set [8]. Depending on the magnitude of the resulting sensitivities, the filter-computed estimation error covariance is modified to account for the unmodeled effects in order to generate a more realistic estimate of predicted navigation performance. The filter has no knowledge about the contribution of the unmodeled parameters to the uncertainty in the state estimate since the modified covariance (the *consider covariance*), which includes effects from both the estimated and consider parameters, is not fed back to the filter. Reduced-order filters of this type have been known to experience *failure modes*, such as cases in which the addition of data yields an increase in the consider covariance, or cases when the consider covariance propagates to an unreasonably large result over time. In these instances, it may be necessary to empirically "tune" the filter (e.g., adjust data weights, model assumptions, etc.) to obtain useful estimates. A mathematical description of these so-called "failure modes" and suggested remedies is described by Scheeres [6].

B. Optimal and Suboptimal Filter Equations

Restricting the discussion to the filter measurement update equations, the mathematical model presented here is the *covariance form* of the measurement update for scalar measurements. Let $\hat{\mathbf{x}}$ represent the state estimate and P represent the error covariance matrix. Using the convention that "(+)" denotes a postmeasurement update value and "(−)" denotes a premeasurement update value, the (optimal) filter measurement update equations for a linear, sequential estimator are given by

$$\text{state estimate} \quad \hat{\mathbf{x}}_k^{(+)} = \hat{\mathbf{x}}_k^{(-)} + \hat{K}_k \left[\mathbf{z}_k - A_{x_k}\hat{\mathbf{x}}_k^{(-)}\right] \quad (1)$$

$$\text{error covariance} \quad P_k^{(+)} = \left[I - \hat{K}_k A_{x_k}\right] P_k^{(-)} \quad (2)$$

$$\text{(optimal) gain matrix} \quad \hat{K}_k = \alpha_k^{-1} P_k^{(-)} A_{x_k}^T \quad (3)$$

where $\mathbf{z}_k$ is the observation vector defined by the measurement model, A_{x_k} is the measurement matrix of observation partial derivatives, I is simply the unit or identity matrix, and $\alpha_k = A_{x_k} P_k^{(-)} A_{x_k}^T + W_k^{-1}$ is the innovations covariance. W_k represents the weighting matrix, the inverse of which is taken to be the diagonal measurement covariance R_k; thus, for $i = 1, \ldots, m$ observations, $W_k^{-1} \equiv R_k = \text{diag}\,[r_1, \ldots, r_m]$ for measurement variances r_i.[4] The filter equations described by Eqs. (1) through (3) can be employed without loss of generality, since "whitening" procedures can be used to statistically decouple the measurements in the presence of correlated measurement noise and obtain a diagonal R_k [7]. The gain matrix K_k is used to update estimates of the filter parameters as each measurement is processed. Note that Eq. (2) is valid only for the optimal gain $\hat{K}_k$.

The use of Eq. (2) to compute the error covariance matrix has historically been suspect due to finite computer word length limitations.[5] As a result, a frequently utilized alternative is the *stabilized Joseph form* of the update, expressed as

$$P_k^{(+)} = (I - K_k A_{x_k})\, P_k^{(-)} (I - K_k A_{x_k})^T + K_k W_k^{-1} K_k^T \quad (4)$$

Although this form of the covariance measurement update is more stable numerically than Eq. (2), it requires a greater number of computations; however, a further advantage is that it is valid for *arbitrary* gain matrices; therefore, K_k in Eq. (4) need not be optimal.

In some cases, the Joseph form of the update may also be deficient numerically [9]. As a result, factorization methods have been developed to help alleviate the numerical deficiencies of the measurement update algorithms [7,10,11]. Specific details of the factorization procedures will not be discussed here; however, an important observation from the literature and critical to the general evaluation mode of the filter is the observation that Eq. (4) can be written in an equivalent form as

[3] This is the more traditional filtering method most often used in practical applications of interplanetary navigation (see introductory remarks), operationally referred to as the *consider option*.

[4] It is assumed that the measurements are corrupted by a vector of independent, zero-mean Gaussian random noise quantities with covariance R_k.

[5] Recall from optimal estimation theory that the error covariance matrix is defined as the expected value of the mean-square estimation error, $P_k \equiv E\left[(\mathbf{x}_k - \hat{\mathbf{x}}_k)(\mathbf{x}_k - \hat{\mathbf{x}}_k)^T\right]$.

$$P_k^{(+)} = \left(I - \hat{K}_k A_{x_k}\right) P_k^{(-)} + \alpha_k \left(K_k - \hat{K}_k\right)\left(K_k - \hat{K}_k\right)^T \tag{5}$$

where K_k is an arbitrary (e.g., suboptimal) gain matrix and $\hat{K}_k$ is the optimal filter gain matrix. This form of the error covariance measurement update is often referred to as the *suboptimal measurement update* since it includes a correction based on the gain difference between the filter evaluation run (which generally assumes an incorrect model) and the original filter (estimation) run. In the genral evaluation mode, the filter uses suboptimal gains saved in an evaluation filter from an earlier filter which is run purposely with what is believed to be an incorrect model, in order to generate suboptimal gains [5]. It is this form of the suboptimal measurement update which will be critical to the error budget development described in the following section. In practice, Eq. (5) is typically mechanized in a *U-D* factorized form for numerical stability. A final note about the filter equations: Although the equations for the time update were not presented, it is important to note that the time update in the general filter evaluation mode takes the same form as the original filter time update, except that in the presence of process noise modeling parameters, the original filter stochastic time constants and process noise uncertainties are replaced with evaluation mode time constants and process noise terms [5].[6]

III. Mission Scenario, Data Acquisition, and Filter Modeling Assumptions

A. Mars Observer Interplanetary Cruise Scenario

The Mars Observer spacecraft was launched successfully on September 25, 1992, and was scheduled to initiate the Mars Orbit Insertion (MOI) burn on August 24, 1993; however, communication with the spacecraft was tragically lost just days prior to MOI. Despite the loss of the spacecraft, the interplanetary cruise phase of the mission, which extended from injection to initiation of the MOI burn, represented a challenging navigation scenario, as the declination of the Mars Observer at encounter was within 1 deg of zero. This is a geometry which has historically yielded relatively poor performance with Doppler tracking, due to Doppler data's relative insensitivity to some components of the spacecraft's state in this regime. The Mars Observer was also the first spacecraft to carry an X-band transponder and the first to rely solely on a single-frequency X-band telecommunications system.[7] Thus, this scenario represents a realistic scenario with which to study the relative merits of using the enhanced orbit determination filter to reduce X-band Doppler and ranging data.

The trajectory segment selected for this analysis was taken to be a 182-day time period extending from early February 1993 to early August 1993, which represented the longest leg of the interplanetary cruise, and had the most stringent navigation accuracy requirements in order to support the final maneuver prior to MOI. The trajectory characteristics over the time span of the data arc, which extended from encounter minus 194 (E − 194) days to E − 12 days, are summarized in Table 1.

B. Data-Acquisition Strategy

A fairly sparse DSN data-acquisition schedule was assumed, containing no more than one or two passes of Doppler and ranging data per week. In all cases, the data were assumed to be acquired from the DSN's 34-m high-efficiency (HEF) Deep Space Stations (DSSs) located near Goldstone, California (DSS 15), Canberra, Australia (DSS 45), and Madrid, Spain (DSS 65). This reduced level of coverage is representative of the level anticipated for telemetry acquisition in future missions such as Pathfinder and Cassini. The data schedule consisted of one horizon-to-horizon tracking pass of two-way Doppler and ranging data acquired from the Madrid site on a weekly basis from E − 194 days to E − 90 days, two weekly tracking passes acquired from the Madrid and Canberra sites from E − 90 days to E − 30 days and from E − 30 days to E − 12 days (data cutoff), and a single pass per day from all three DSN sites.

To account for data noise, an assumed one-sigma random measurement uncertainty of 0.0126 mm/sec was chosen for two-way Doppler, and for two-way ranging, the one-sigma random measurement uncertainty was assumed to be 1 m; these noise variances were used in all cases in a manner similar to an earlier study [2]. It should be noted that the data weights quoted here are for the round-trip range-rate and range, respectively. Both data types were collected at a rate of one point every 10 min, and the noise variances were adjusted by an elevation-dependent function for all stations, to reduce the weight of the low-elevation data; furthermore, no data were acquired at elevations of less than 10 deg.

[6] The software is described in S. C. Wu, W. I. Bertiger, J. S. Border, S. M. Lichten, R. F. Sunseri, B. G. Williams, P. J. Wolff, and J. T. Wu, *OASIS Mathematical Description*, V. 1.0, JPL D-3139 (internal document), Jet Propulsion Laboratory, Pasadena, California, April 1, 1986.

[7] P. B. Esposito, S. W. Demcak, D. C. Roth, W. E. Bollman, and C. A. Halsell, *Mars Observer Project Navigation Plan*, Project Document 642-312, Rev. C (internal document), Jet Propulsion Laboratory, Pasadena, California, June 15, 1990.

C. Orbit Determination Filter Model

Table 2 summarizes the parameters which make up the enhanced orbit determination filter model, along with a priori statistics, steady-state uncertainties for the Gauss–Markov parameters, and noise densities for the random-walk parameters.[8] All of the parameters were treated as filter (estimated) parameters and grouped into three categories: spacecraft epoch state, spacecraft nongravitational force model, and ground system error model. Effects of uncertainty in the ephemeris and mass of Mars were neglected, as they were believed to be relatively small in this scenario.[9]

The simplified spacecraft nongravitational force model was based on past experience and modeling spacecraft similar to Mars Observer.[10] There were filter parameters representing solar radiation pressure forces as well as small anomalous forces due to gas leaks from valves and pressurized tanks, attitude control thruster misalignments, etc. For processing the two-way ranging data, the filter model included a stochastic bias parameter associated with each ranging pass from each station, in order to approximate the slowly varying, nongeometric delays in ranging measurements that are caused principally by station delay calibration errors and uncalibrated solar-plasma effects. No explicit model parameters were employed for the effect of solar-plasma delays as relatively large (>45 to 60 deg) Sun–Earth–Probe (SEP) angles were assumed for ranging data acquisition, leading to small (<1 m) solar plasma delays.[11]

The station location covariance represents the uncertainty in the station location and pole model solutions developed by Finger and Folkner [13]; this covariance matrix and its associated station location set were used operationally by the Mars Observer Navigation Team during interplanetary cruise.[12] Additionally, three exponentially correlated process noise parameters were included to account for the dynamical uncertainties in the Earth's pole location and rotation period. The tropospheric and ionospheric zenith delay calibration uncertainties were representative of current calibration accuracy. A sequential *U-D* factorized estimation scheme was employed, in order to track the short-term fluctuations in the transmission media.

IV. Error Budget Calculations

The purpose of developing an error budget is to determine the contribution of individual error sources, or groups of error sources, to the total navigational uncertainty. In general, an error budget is a catalog of the contributions of *all* of the error sources which contribute to errors in the filter estimate at a particular point in time, whether explicitly modeled in the filter or not [3]. For this first analysis, it is assumed that the filter is "optimal," i.e., that the truth model and filter model are the same. This implies that the filter model is an accurate representation of the physical world.

In order to establish an error budget, it is necessary to compute a time history of the filter gain matrix for the *complete* filter model and to subsequently use these gains in the sensitivity calculations [Eq. (4)] during repeated filter evaluation mode runs, in which only selected error sources or groups of error sources are "turned on" in each particular run. In this way, the individual contributions of each error source or group of error sources to the total statistical uncertainty obtained for all of the filter parameters for a given radio metric data set can be established.

Using the reduced data schedule and enhanced filter model derived for the Mars Observer interplanetary cruise scenario described in Section III, orbit determination error statistics were computed for DSN Doppler-only, ranging-only, and Doppler-plus-ranging data sets. The orbit determination statistics were propagated to the nominal time of Mars encounter and expressed as dispersions in a Mars-centered aiming plane, or B-plane, coordinate system;[13]

[8] For process noise, first-order Gauss-Markov (exponentialy correlated) random processes were assumed. The process noise covariance is given by $q = (1 - m^2)\sigma_{ss}^2$ where $m = \exp[-(t_{j+1} - t_j)/\tau]$. Here, t_j is the start time for the jth batch and τ is the associated time constant. The term σ_{ss} is the steady-state uncertainty, i.e., the noise level that would be reached if the dynamical system were left undisturbed for a time much greater than τ. For the random walk, both σ_{ss} and τ are unbounded ($\tau = \infty$) and a steady-state is never reached. The noise density for the random walk is characterized by the rate of change of the process noise covariance, $q = \Delta q/\Delta t$ where Δt is the batch size and Δq is the amount of noise added per batch. For this analysis, $\Delta t = 10$ min.

[9] E. M. Standish, "Updated Covariance of Mars for DE234," JPL Interoffice Memorandum 314.6-1452 (internal document), Jet Propulsion Laboratory, Pasadena, California, July 27, 1992.

[10] Esposito, op. cit.

[11] A recent study of a simple solar plasma delay model and its use in the reduction of precision ranging data is presented in [12].

[12] W. M. Folkner, "DE234 Station Locations and Covariance for Mars Observer," JPL Interoffice Memorandum 335.1-92-013 (internal document), Jet Propulsion Laboratory, Pasadena, California, May 26, 1992.

[13] The aiming plane, or B-plane, coordinate system is defined by three unit vectors: $\underline{\mathbf{S}}$, $\underline{\mathbf{T}}$, and $\underline{\mathbf{R}}$; $\underline{\mathbf{S}}$ is parallel to the spacecraft velocity vector relative to Mars at the time of entry into Mars' gravitational sphere of influence, $\underline{\mathbf{T}}$ is parallel to the Martian equatorial plane, and $\underline{\mathbf{R}}$ completes an orthogonal triad with $\underline{\mathbf{S}}$ and $\underline{\mathbf{T}}$. The aim point

specifically, the one-sigma magnitude uncertainty of the miss vector, resolved into the respective miss components $\mathbf{B}\bullet\underline{\mathbf{R}}$ (normal to Martian equatorial plane) and $\mathbf{B}\bullet\underline{\mathbf{T}}$ (parallel to Martian equatorial plane), and the one-sigma uncertainty in the *linearized time-of-flight* (LTOF). The LTOF defines the time from encounter (point of closest approach) and specifies what the time of flight to encounter would be if the magnitude of the miss vector were zero. In some cases, the errors were expressed as dispersion ellipses in the B-plane to graphically illustrate the contributions of the most statistically significant groups of error sources.

A. Doppler Only

With the enhanced filter, the Doppler data allowed determination of the $\mathbf{B}\bullet\underline{\mathbf{R}}$ component of the miss vector to about 22 km and the $\mathbf{B}\bullet\underline{\mathbf{T}}$ component to about 46 km, with the LTOF determined to approximately 7 sec (~16 km in positional uncertainty). These results are summarized in Table 3, which gives the magnitude of the B-plane dispersions around the nominal MOI aim point (in the form of an error budget) for all groups of truth/filter model error sources to the total statistical uncertainty, in a root-sum-square sense. (Recall that for this analysis, the truth model and filter model are the same.) As seen from the table, the most dominant error source groups were the random nongravitational accelerations, followed by solar radiation pressure coefficient uncertainty, and random Earth-orientation calibration errors. A graphical illustration of these contributions is shown in Fig. 1, in terms of B-plane dispersion ellipses. For this encounter scenario, the direction of the Earth–spacecraft range is closely aligned with the semimajor axis of the B-plane dispersion ellipse. The Doppler data alone were able to determine this component of the solution to only about 50 km.

B. Ranging Only

Orbit solutions computed with ranging data using the enhanced filter are summarized in Table 4, also in error budget format. In this case, the ranging data were able to determine the $\mathbf{B}\bullet\underline{\mathbf{R}}$ component of the miss vector to about 12 km and the $\mathbf{B}\bullet\underline{\mathbf{T}}$ component to about 6 km. The LTOF accuracy for this case was not much better than the Doppler-only case, an improvement from 7 sec to approximately 6 sec (~14 km in positional uncertainty). The most dominant error source groups for this data strategy were random nongravitational accelerations, as in the Doppler-only case, followed by measurement (data) noise, and DSN station location uncertainty. Although range bias parameters were included in the ground system error model, they did not adversely affect the performance of the enhanced filter. Figure 2 illustrates these major error sources in terms of B-plane dispersion ellipses along with the full filter-generated root-sum-square uncertainty. The orientation of the full filter dispersion ellipse is rotated about 90 deg from the Doppler-only result, indicating the strength with which the ranging data are able to determine the Earth–spacecraft range component of the trajectory. In this case, the semimajor axis is oriented roughly normal to the Earth–Mars line.

C. Doppler Plus Ranging

For the final case in which both Doppler and ranging data were used, the $\mathbf{B}\bullet\underline{\mathbf{R}}$ component of the miss vector was determined to about 9 km and the $\mathbf{B}\bullet\underline{\mathbf{T}}$ component to about 5 km, with the LTOF determined to approximately 4 sec (~9 km in positional uncertainty). Error budget calculations for this case are summarized in Table 5. Similar to the results for the Doppler-only and ranging-only data strategies, random nongravitational accelerations were the dominant error source group. The next two most significant error source groups were Earth-orientation calibration error and DSN station location uncertainty, respectively. As with the ranging-only case, solar radiation pressure coefficient uncertainty and random ranging delay calibration errors were of roughly the same magnitude, but did not contribute to the total error budget as much as the previously cited error sources. B-plane dispersion ellipses are also provided (see Fig. 3), illustrating the contributions of the major error source groups to the total root-sum-square error and the orientation of the ellipses in the aiming plane. In this case, the accuracy with which the Earth–spacecraft range component at encounter was determined was roughly 11 km.

V. Sensitivity Curves

Another benefit of the linearity assumptions used to develop error budgets is that sensitivity curves can readily be generated. *Sensitivity curves* graphically illustrate the effects of using different prescribed values of the error source statistics on the estimation errors, with the assumption that the filter model remains unchanged. The procedure for sensitivity curve development is straightforward and, although described in [3], is repeated here for completeness: (1) subtract the contribution of the error source under consideration from the total mean-square navigation error; (2) to compute the effect of changing the error source by a preset scale factor, multiply its contributions to the mean-square errors by the square of the scale factor value; (3) replace the original contribution to mean-square error

for planetary encounter is defined by the miss vector $\mathbf{B}$, which lies in the $\underline{\mathbf{T}}-\underline{\mathbf{R}}$ plane and specifies where the point of closest approach would be if the target planet had no mass and did not deflect the flight path.

by the one computed in the previous step; and (4) take the square root of the newly computed mean-square error to obtain the total root-sum-square navigation error.

Several cases were used to generate sensitivity curves for the major groups of error sources in the filter model; for example, Figs. 4 through 6 give the sensitivity curves for the random nongravitational accelerations and illustrate the sensitivity of this error source group to various scale factor values. Recall that random nongravitational accelerations dominated the error budget in all three data strategy cases considered (c.f., Section IV). As seen from the figures, a quadratic growth in the sensitivity is evident for scale factor values ranging from 1 to 3, and a nearly linear growth is exhibited for scale factor values ranging from 4 to 10. On average, for all three data strategies considered, an order of magnitude increase in the preset scale factor resulted in about a factor of three to six increase in the root-mean-square estimation errors.

VI. Summary and Conclusions

A sensitivity analysis was conducted for a recently developed sequential data filtering strategy referred to as the *enhanced orbit determination filter.* In practice, the enhanced filter attempts to represent all or nearly all of the principal ground system error sources affecting radio metric data types as filter parameters. Reduced-order filtering methods were reviewed and utilized to perform the sensitivity analysis, and, in particular, to develop navigation error budgets for three different data acquisition strategies. The mission scenario assumed for the analysis was based on the Mars Observer interplanetary outer cruise phase. Two-way radio Doppler and ranging were the data types analyzed, with assumed accuracies chosen to reflect actual performance of the DSN's X-band tracking system, as observed in recent interplanetary missions such as Magellan, Ulysses, and Mars Observer.

Error budget computations performed for the assumed mission scenario revealed that the most significant error source for all three data-acquisition strategies studied (i.e., Doppler-only, ranging-only, and Doppler-plus-ranging) was spacecraft random nongravitational accelerations, indicating that, for the reference error model, the enhanced filter is most sensitive to mismodeling of small anomalous forces affecting the spacecraft. Other sources of error which had a significant impact on the overall error budget were, in the case of Doppler-only navigation, solar-radiation pressure coefficient uncertainty and Earth-orientation calibration error. In the case of ranging-only navigation, measurement noise and Earth-orientation calibration error were the other significant contributors to the overall error budget. Earth platform errors, namely DSN station location uncertainty and Earth-orientation calibration error, were the next most significant contributors to the overall error budget for the Doppler-plus-ranging navigation case. These results suggest that if high-precision navigation performance is to be achieved, the error sources requiring the most accurate modeling are spacecraft nongravitational accelerations and Earth platform calibration errors. Future work will focus on the use of Monte Carlo simulation techniques to evaluate the sensitivity of the enhanced orbit determination filter to a variety of truth model assumptions, and will include additional model parameters to account for trajectory-correction maneuver execution errors and uncalibrated solar-plasma delays.

Acknowledgments

The authors would like to thank Sam Thurman of JPL and Robert Bishop of The University of Texas at Austin for their valuable input, support, and review of this article.

References

[1] S. W. Thurman and J. A. Estefan, "Radio Doppler Navigation of Interplanetary Spacecraft Using Different Data Processing Modes," paper AAS 93-163, presented at the AAS/AIAA Spaceflight Mechanics Meeting, Pasadena, California, February 22-24, 1993.

[2] J. A. Estefan, V. M. Pollmeier, and S. W. Thurman, "Precision X-Band Doppler and Ranging Navigation for Current and Future Mars Exploration Missions," paper AAS 93-250, presented at the AAS/GSFC International Symposium on Space Flight Dynamics, Greenbelt, Maryland, April 26–30, 1993.

[3] *Applied Optimal Estimation*, edited by A. Geld, Cambridge, Massachusetts: M.I.T. Press, pp. 229–230 and 260–266, 1974.

[4] P. S. Maybeck, *Stochastic Models, Estimation, and Control: Volume 1*, San Diego, California: Academic Press, Inc., pp. 325–327 and 337–341, 1979.

[5] S. M. Lichten, "Estimation and Filtering Techniques for High-Accuracy GPS Applications," *The Telecommunications and Data Acquisition Progress Report 42-97, vol. January-March 1989*, Jet Propulsion Laboratory, Pasadena, California, pp. 1–20, May 15, 1989.

[6] D. J. Scheeres, "Failure Modes of Reduced-Order Orbit Determination Filters and Their Remedies," *The Telecommunications and Data Acquisition Progress Report 42-114, vol. April-June 1993*, Jet Propulsion Laboratory, Pasadena, California, pp. 34–42, August 15, 1993.

[7] G. J. Bierman, *Factorization Methods for Discrete Sequential Estimation*, San Diego, California: Academic Press, Inc., pp. 162–171, 1977.

[8] S. R. McReynolds, "The Sensitivity Matrix Method for Orbit Determination Error Analysis, With Applications to a Mars Orbiter," *JPL Space Programs Summary 37-56*, vol. 3, January–February 1969, pp. 85–87, March 31, 1969.

[9] G. J. Bierman and C. L. Thornton, "Numerical Comparison of Kalman Filter Algorithms: Orbit Determination Case Study," *Automatica*, vol. 13, pp. 23–35, 1977.

[10] C. L. Thornton, "Triangular Covariance Factorizations for Kalman Filtering," JPL Technical Memorandum 33-798, Jet Propulsion Laboratory, Pasadena, California, October 15, 1976.

[11] C. L. Thornton and G. J. Bierman, "Filtering and Error Analysis Via the UDU^T Covariance Factorization," *IEEE Trans. on Automatic Control*, vol. AC-23, no. 5, pp. 901–907, 1978.

[12] T. P. McElrath, S. W. Thurman, and K. E. Criddle, "Navigation Demonstrations of Precision Ranging with the Ulysses Spacecraft," paper AAS 93-687, presented at the AAS/AIAA Astrodynamics Specialist Conference, Victoria, B.C., Canada, August 16–19, 1993.

[13] M. H. Finger and W. M. Folkner, "A Determination of the Radio-Planetary Frame Tie From Comparison of Earth Orientation Parameters," *The Telecommunications and Data Acquisition Progress Report 42-109, vol. January-March 1992*, Jet Propulsion Laboratory, Pasadena, California, pp. 1–21, May 15, 1992.

Table 1. Mars Observer outer cruise phase trajectory characteristics over an assumed data arc extending from E — 194 days to E — 12 days.

Parameter	Value
Earth-to-spacecraft range, km	80×10^6 to 330×10^6
Geocentric declination, deg	22 to 1
SEP angle, deg	125 to 45

Table 2. Enhanced orbit determination filter with ground-system error model representative of current DSN calibration accuracy.

Estimated parameter set	Uncertainty (1σ)	Remarks
Spacecraft epoch state	A priori,	
Position components	10^5 km	Constant
Velocity components	1 km/sec	parameters
Nongravitational force model		
Solar radiation pressure	A priori,	
Radial (G_r)	10% (= 0.13)	Constant
Transverse (G_x/G_y)	10% (= 0.01)	parameters
Anomalous accelerations	Steady-state,	Markov parameters
Radial (a_r)	10^{-12} km/sec^2	10-day time constant
Transverse (a_x/a_y)	10^{-12} km/sec^2	10-day time constant
Range biases (one per station per pass, ranging data only)	A priori, 4 m	Uncorrelated from pass to pass
Ground system error model		
DSN station locations	A priori,	Constant parameters,
Spin radius (r_s)	0.18 m	relative uncertainty
Z-height (z_s)	0.23 m	between stations is
Longitude (λ)	3.6×10^{-8} rad	1 to 2 cm
Earth orientation	Steady-state,	Markov parameters,
Pole orientation	1.5×10^{-8} rad	1-day time constant
Rotation period	0.2 msec	12-hr time constant
Transmission media	A priori,	Random walk,
Zenith troposphere (each station)	5 cm	1 cm^2/hr
Zenith ionosphere (each station)	Steady-state, 3 cm	Markov parameters 4-hr time constant

Table 3. Enhanced-filter error budget for DSN X-band Doppler-only navigation.

Error source group	B-plane dispersions		
	$\mathbf{B}\bullet\underline{\mathbf{R}}$, km	$\mathbf{B}\bullet\underline{\mathbf{T}}$, km	LTOF, sec
Epoch state	2.92	8.33	0.753
SRP parameters	10.25	27.69	2.164
Nongravitational accelerations	16.52	30.61	4.950
Ionosphere	1.87	3.82	0.891
Troposphere	3.56	6.65	1.500
Station locations	4.29	4.63	1.590
Earth orientation	6.23	14.58	3.428
Measurement noise	3.45	6.41	1.501
Total (root-sum-square)	21.72	45.90	7.024

Table 4. Enhanced-filter error budget for DSN X-band ranging-only navigation.

Error source group	B-plane dispersions		
	$\mathbf{B}\bullet\underline{\mathbf{R}}$, km	$\mathbf{B}\bullet\underline{\mathbf{T}}$, km	LTOF, sec
Epoch state	0.27	0.13	0.23
SRP parameters	2.26	1.11	0.91
Nongravitational accelerations	7.27	3.54	4.13
Ionosphere	0.78	0.39	0.27
Troposphere	1.54	0.75	0.64
Station locations	5.36	2.63	2.66
Earth orientation	2.47	1.26	0.63
Range biases	2.06	1.00	0.97
Measurement noise	6.59	3.21	3.18
Total (root-sum-square)	11.98	5.86	6.08

Table 5. Enhanced-filter error budget for DSN X-band Doppler-plus-ranging navigation.

Error source group	B-plane dispersions		
	$\mathbf{B}\bullet\underline{\mathbf{R}}$, km	$\mathbf{B}\bullet\underline{\mathbf{T}}$, km	LTOF, sec
Epoch state	0.10	0.05	0.10
SRP parameters	1.57	0.76	0.64
Nongravitational accelerations	5.73	2.83	2.87
Ionosphere	0.87	0.41	0.56
Troposphere	1.46	0.69	0.81
Station locations	2.99	1.53	0.97
Earth orientation	2.98	1.50	1.26
Range biases	1.40	0.67	0.68
Measurement noise	5.11	2.46	2.51
Total (root-sum-square)	9.17	4.51	4.35

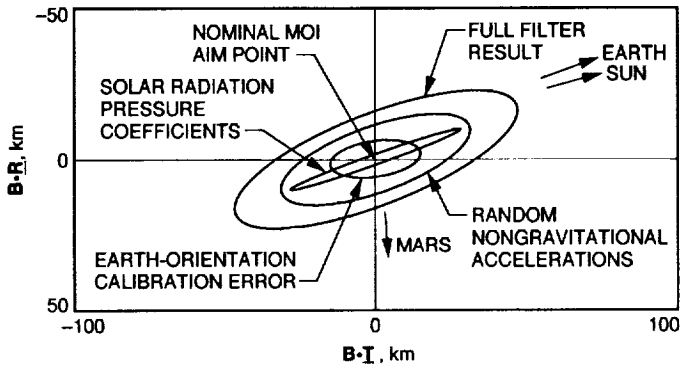

Fig. 1. Mars Observer aiming plane dispersions (one sigma) for DSN X-band Doppler-only navigation.

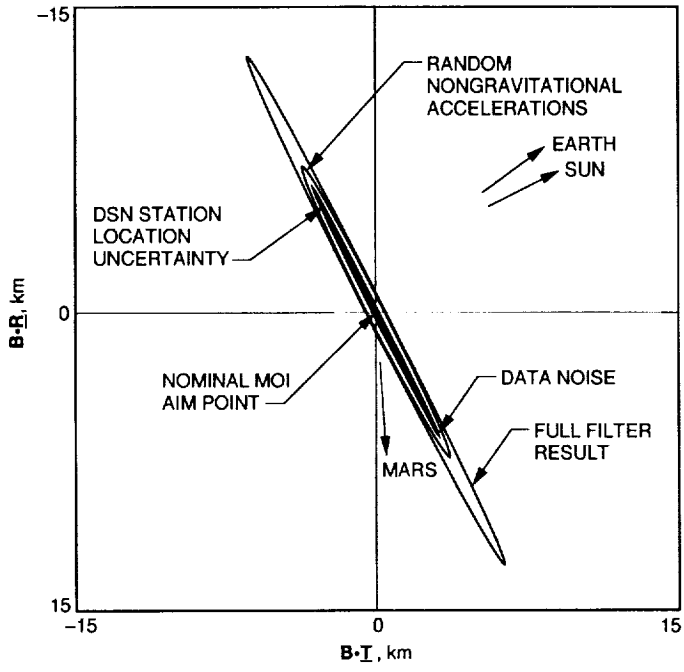

Fig. 2. Mars Observer aiming plane dispersions (one sigma) for DSN X-band ranging-only navigation.

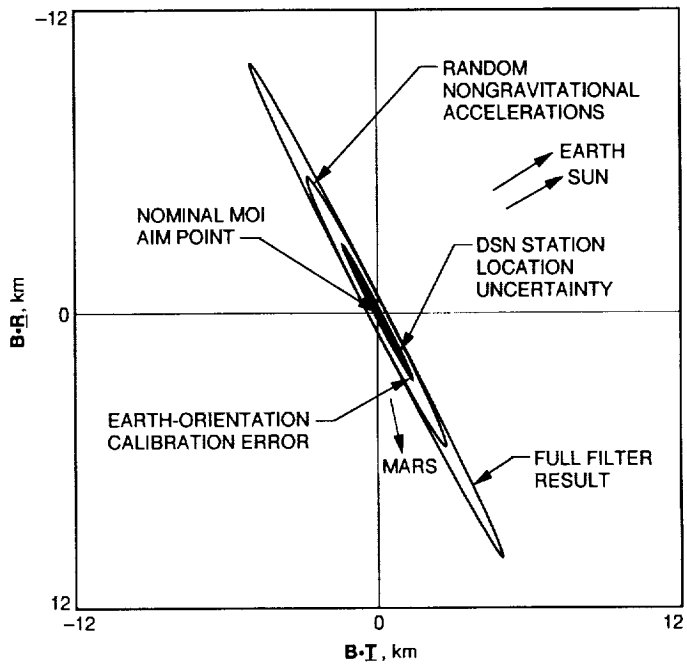

Fig. 3. Mars Observer aiming plane dispersions (one sigma) for DSN X-band Doppler-plus-ranging navigation.

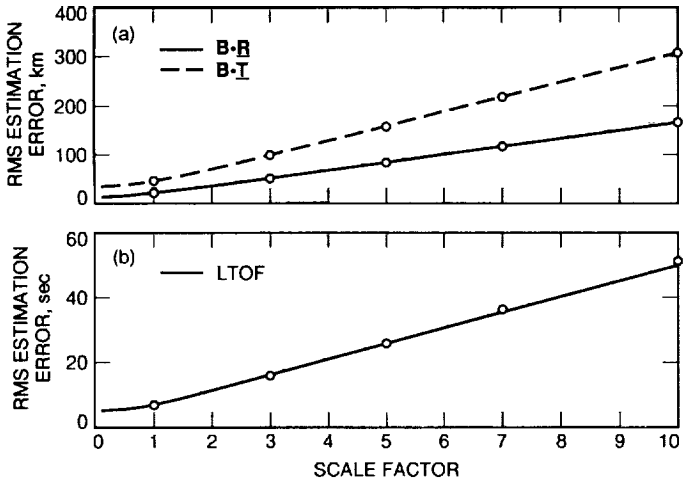

Fig. 4. Sensitivity of root-mean-square estimation error to perturbations of random nongravitational accelerations by preset scale factor (Doppler-only case): (a) B•T and B•R and (b) LTOF.

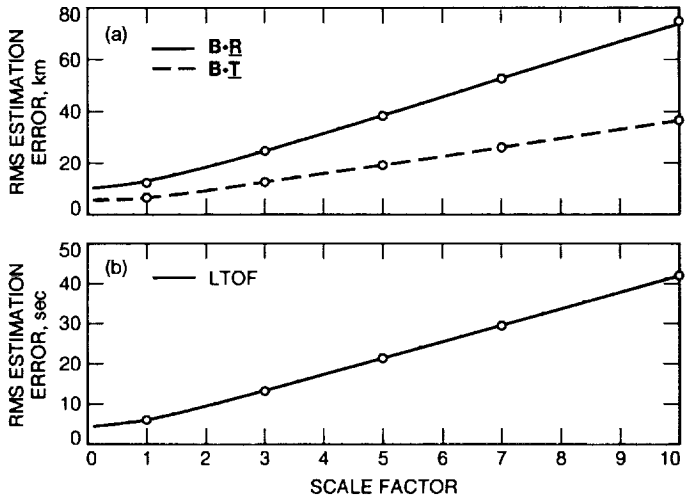

Fig. 5. Sensitivity of root-mean-square estimation error to perturbations of random nongravitational accelerations by preset scale factor (ranging-only case): (a) B•T and B•R and (b) LTOF.

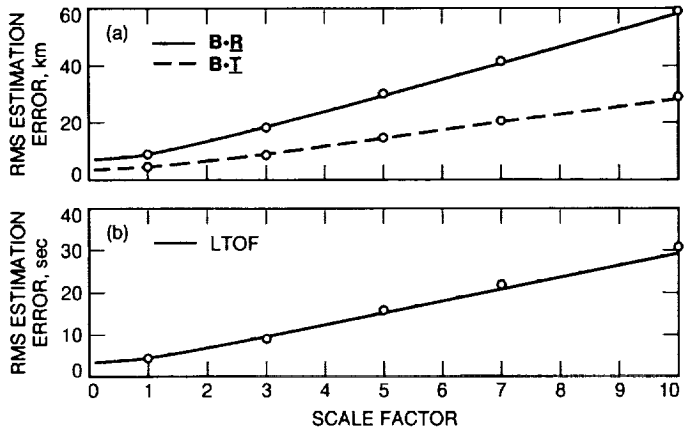

Fig. 6. Sensitivity of root-mean-square estimation error to perturbations of random nongravitational accelerations by preset scale factor (Doppler-plus-ranging case): (a) B•T and B•R and (b) LTOF.